State space analysis of ocean surface warming on decadal scale

K. S. Yajnik

CSIR Fourth Paradigm Institute, Wind Tunnel Road, Bengaluru 560 037, India

Detection of small decadal-scale variation amidst larger variations on smaller timescales is carried out here by geometrical segregation rather than filtering. Sea surface temperature (SST) annual cycle is represented as a point in a 12-dimensional space and thermal history as a path connecting successive points. Drift of the domain of decadal variations in the state space is taken as a measure of change from one decade to another. Visualization of the path in the 12-dimensional space is achieved by projecting it on planes. A matrix transformation gives an orthogonal decomposition of the annual cycle resembling Fourier series. The specific problem investigated here is the response of the Northern, the Tropical and the Southern Oceanic Regions (NOR, 30°–90°N; TOR, 30°S–30°N; SOR, 90°–30°S) to global warming during 1951–2010. The results are based on the Extended Reconstructed Sea Surface Temperature version 4 (ERSSTv4) database. Several interesting findings are obtained. The decadal scale warming has a seasonal variation, the largest being in the NOR (~0.26°C to ~0.57°C), in 2001–10. The consequential change in the annual cycle is increase in the amplitude of the annual mode in addition to increase in the annual mean. Decade-on-decade SST increase has peaked first in the SOR in 1971–80, and last in the NOR in 2001–10.

Keywords: Normal modes, ocean warming, seasonal cycle, sea surface temperature, state space analysis.

THE ocean surface temperature is well known as an important parameter for climate studies, not only because the ocean covers nearly 71% of the earth surface and is the dominant reservoir of heat, but also because sea surface temperature (SST) gradient is known to be a key forcing in the dynamics of the atmosphere and the ocean. In the present work, the world ocean is divided into three regions, the Tropical Oceanic Region (TOR) in low latitudes, which is surplus in net annual radiation, and two regions in middle-to-high latitudes, the Northern (NOR) and the Southern Oceanic Regions (SOR), both of which are deficit in net annual radiation[1,2]. Their response to global warming is analysed in terms of decadal-scale changes in the spatial averages of SST over them. The temperature differences between the former region and the latter two regions are the primary drivers of global meridional circulation, and therefore the key determinants of the seasonal pole-ward heat transports in the atmosphere and the oceans. The motivation for the present investigation is to obtain insight into the role of the horizontal advective processes in modulating the effects of the vertical heat transfer processes, as the former have not been investigated as extensively as the latter in elucidating the effects of rising greenhouse gases (GHGs) on the earth surface temperature.

The starting point of the present analysis is the view that, in climate studies, the annual thermal cycle should be considered holistically, as it is the annual rhythm which regulates the life of flora and fauna on earth. The simplest way to do it is to represent the annual cycle geometrically as a point in the 12-dimensional space of monthly SSTs. Thus an N-year long record is represented as the path connecting successive N state points. A segment of the path linking the points of a decade then represents the SST climate in that decade. The envelope (in a projection on a plane, it is a rectangle with sides parallel to monthly SST axes) enclosing a decadal path segment represents the domain of variation of SST during the decade and is called the decadal envelope. Its drift indicates changes on decadal timescale and its deformation is an index of decadal change in inter-annual variability. Also, the transformation given in the next section offers a 'frequency domain view', that is, an orthogonal decomposition of the annual cycle similar to Fourier series.

The author has devised the present method, as available methods like sliding 30-year averages seem to have the disadvantage of attenuating and distorting small decadal variation in the presence of larger variations on interannual and seasonal scales. Wavelet methods are well suited for high-frequency time-localized events, but they seem inappropriate when the signal is secular or of ultra-low frequency, and is not localized in time. The author's ideas have evolved slowly over several years. An early version was presented at a conference in 2013 (ref. 3).

The results reported here are based on Extended Reconstructed Sea Surface Temperature version 4 (ERSSTv4)[4,5]. A brief comparison of the results with those obtained from ERSSTv3b (refs 6–11) and HadISSTv1.1 (ref. 12) is also given. A few general comments on SST datasets are given here; for further information the readers are referred to the original papers[4–12].

e-mail: ksy@csir4pi.in

These datasets have to address four major issues: sparse data in several periods before 1950, objective correction methods for bias errors arising from diverse SST measuring methods (use of un-insulated/insulated bucket on ship deck, engine intake temperature, buoy mounted thermistor, AVHHR data, etc.), minimizing high-frequency noise, and correction for the presence of ice in seawater in polar regions[4–12].

The plan of the article is to introduce the basic concepts in the next section. The subsequent section presents the results based on ERSSTv4. First, interpretation of the drift of decadal envelopes of SST is given. Then follows a brief comparison with results from two other datasets. The section also contains application of the method to difference between SST of adjacent regions and to warm pool area in TOR. The next section gives a brief discussion of a hypothesis that seeks to explain seasonal aspects of warming in middle-to-high latitudes. The final section summarizes major conclusions.

The method

SST data at a location are traditionally given as a time series of monthly mean temperatures. One can take advantage of the rather regular annual cycle by writing 12 series, one for each month, or equivalently a time series of 12-dimensional column vectors $\boldsymbol{T}_n$. Their components T_{mn} denote SST of the mth month of the nth year (m = 1, 2,…,12; n = 1, 2, …, N). T_{mn} can also be considered as the mth coordinate of a point representing the annual cycle of the nth year in a 12-dimensional space. Thermal history is then represented as a path connecting successive points. It can be visualized by its projection on two-dimensional subspaces or planes. Figure 1 *a* and *b*, for example, shows the SST trajectory of the NOR for the period 1951–2010 projected on two planes, June–December and March–September, which are termed solstice and equinox planes. Since the origin in the figure is chosen as the 1951–1980 climatology, the coordinates of a point are monthly SST anomaly (SSTA).

Fourier analysis of climatological cycles has been used in oceanography as it enables one to focus attention on a few dominant normal modes that account for most of the seasonal variance[13]. The transformation given here extends this facility to annual cycles. It rotates and stretches the SST axes and yields a new set of orthogonal axes. It yields an apparatus of normal modes, similar to Fourier modes, but whose coefficients can vary from year to year. This allows one to determine how anomalies in a given year affect the amplitude and the phase of various modes of the annual cycle.

Consider the linear transformation $\mathbf{F}$ relating $\boldsymbol{T}_n$ to the coefficient vectors $\boldsymbol{c}_n$ by

$$\boldsymbol{T}_n = \mathbf{F}\boldsymbol{c}_n, \tag{1}$$

where the elements F_{ij} of the 12 × 12 matrix $\mathbf{F}$ are defined as: $F_{i1} = 1$; for even $j(= 2k < 12)$, $F_{ij} = \sqrt{2}\cos(ik\pi/6)$; for odd $j(= 2k + 1 < 12)$, $F_{ij} = \sqrt{2}\sin(ik\pi/6)$; and $F_{i12} = (-1)^i$ (Table 1). Since $\mathbf{F}^{\mathrm{T}}\mathbf{F} = 12\mathbf{I}$, it follows that

$$\boldsymbol{c}_n = \frac{1}{12}\mathbf{F}^{\mathrm{T}}\boldsymbol{T}_n. \tag{2}$$

The above two equations give an orthogonal decomposition of the annual cycle. Note that the even column vectors of F_{ij} ($j = 2k < 12$) are proportional to discretized cosine functions of frequency k cycles per year (cy^{-1}), and the odd column vectors ($1 < j = (2k + 1) < 12$) are proportional to discretized sine functions of frequency k cy^{-1} ($k < 6$). The last column vector is the discretized cosine function of frequency 6 cy^{-1}. The column vectors are evidently orthogonal. The planes spanned by even and odd column vectors for frequency k cy^{-1} ($1 \le k \le 5$) are called planes of kth mode. Thus there are five regular normal modes of frequencies ranging from 1 to 5 cy^{-1}, and two degenerate normal modes of 0 and 6 cy^{-1}. Equation (1) can also be written as:

$$T_{mn} = c_{1n} + \sqrt{2}\sum_k \left[c_{(2k)n}\cos\left(\frac{mk\pi}{6}\right) + c_{(2k+1)n}\sin\left(\frac{mk\pi}{6}\right)\right] + (-1)^m c_{12n}, \tag{3}$$

where the summation is from k = 1 to 5. The above relation resembles the Fourier series for a periodic function having frequencies up to six, which can be seen by setting $a_{0n} = c_{1n}$, and for $1 \le k \le 5$, $a_{kn} = \sqrt{2}c_{(2k)n}$, $b_{kn} = \sqrt{2}c_{(2k+1)n}$, and $a_{6n} = c_{12n}$. Note however there is no sine term for k = 6. Also, eq. (2) corresponds to the expressions for Fourier series coefficients, except that sums appear instead of integrals. Equations (1) and (2) may be viewed as discrete variants of Fourier series and the components c_{jn} of the vector $\boldsymbol{c}_n$ as normalized Fourier coefficients for the nth year (see Appendix 1).

In the present methodology, changes on scales larger than a year appear as changes in coefficients, and the seasonal cycle is decomposed into normal modes, similar to Fourier modes. This hybrid approach has a major advantage. Since the time series need not be stationary, the method can be used during climate transitions and in extreme events. Since the coefficients vary from year to year, the present modes are termed as annually modulated normal modes (AMNM).

The annual variance of SST can be written as

$$\sigma^2(\boldsymbol{T}_n) = \frac{1}{12}(\boldsymbol{T}_n^{\mathrm{T}}\boldsymbol{T}_n) - a_{0n}^2 = \boldsymbol{c}_n^{\mathrm{T}}\boldsymbol{c}_n - c_{1n}^2. \tag{4}$$

It is expedient to introduce normalized amplitude r_{kn} $(= [c_{(2k)n}^2 + c_{(2k+1)n}^2]^{1/2} = [(a_{kn}^2 + b_{kn}^2)/2]^{1/2}$, and phase

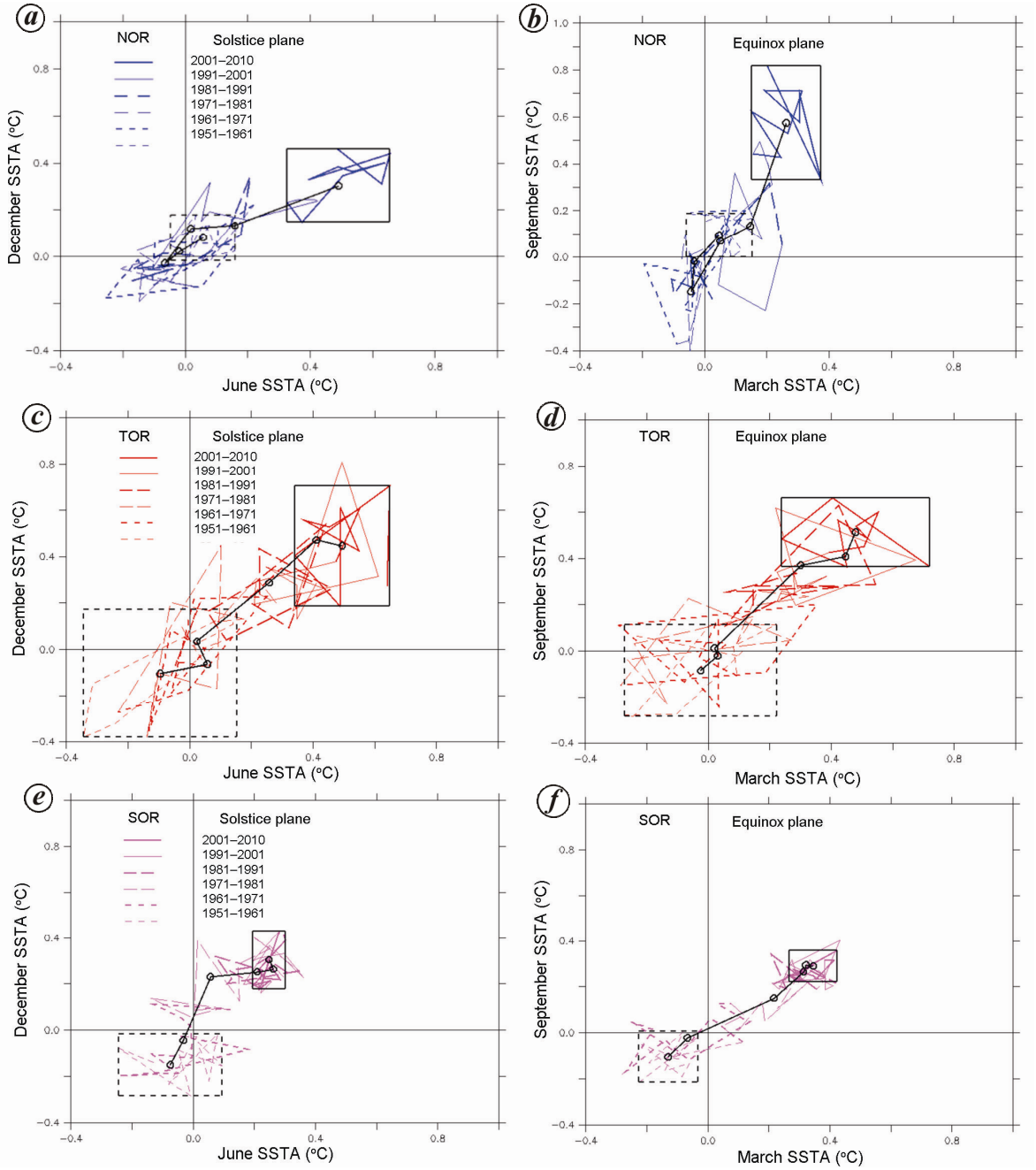

Figure 1 ***a–f.*** Sea surface temperature anomaly (SSTA) trajectories projected on solstice and equinox planes. The origin is at 1951–1980 climatology. Blue, red and light blue colours indicate the Northern (NOR), the Tropical (TOR) and the Southern Oceanic Regions (SOR). Black rectangles indicate decadal envelopes in 1951–60 (dotted lines) and 2001–10 (full lines). Paths of decadal envelope centres (black circles) indicate drift from the origin in the state space. Figures 1, 3–5 are based on the database ERSST v4 (refs 4, 5).

ϕ_{kn} ($k\phi_{kn} = \cos^{-1}(c_{(2k)n}/r_{kn})$, if $c_{(2k+1)n} \geq 0$, else $-\cos^{-1} \times (c_{(2k)n}/r_{kn})$) of the kth mode for k up to 5, and $r_{6n} = c_{12n}$, $\phi_{6n} = 0$. Then the above relation can be written as

$$\sigma^2(\boldsymbol{T}_n) = \sum_{k=1}^{6} r_{kn}^2. \tag{5}$$

Let $\hat{\boldsymbol{T}}_{Kn}$ be an approximation whose coefficient vector $\hat{\boldsymbol{c}}_n$ has all terms for modes of frequency up to frequency K, the same as $\boldsymbol{c}_n$, and the higher mode terms as zero. Let $\boldsymbol{\varepsilon}_{Kn} (= \boldsymbol{T}_n - \hat{\boldsymbol{T}}_{Kn})$ be the error vector. Then the only non-zero components of $\boldsymbol{\varepsilon}_{Kn}$ are for modes higher than K. Then the above relation shows that

$$\sigma^2(\boldsymbol{T}_n) = \sigma^2(\hat{\boldsymbol{T}}_{Kn}) + \sigma^2(\boldsymbol{\varepsilon}_{Kn}). \tag{6}$$

So the variance of the error vector is the contribution of modes of frequency greater than K (see Appendix 1).

Table 1. Elements of the matrix **F**

j	1	2	3	4	5	6	7	8	9	10	11	12
i												
1	1	$\sqrt{3/2}$	$1/\sqrt{2}$	$1/\sqrt{2}$	$\sqrt{3/2}$	0	$\sqrt{2}$	$-1/\sqrt{2}$	$\sqrt{3/2}$	$-\sqrt{3/2}$	$1/\sqrt{2}$	−1
2	1	$1/\sqrt{2}$	$\sqrt{3/2}$	$-1/\sqrt{2}$	$\sqrt{3/2}$	$-\sqrt{2}$	0	$-1/\sqrt{2}$	$-\sqrt{3/2}$	$1/\sqrt{2}$	$-\sqrt{3/2}$	1
3	1	0	$\sqrt{2}$	$-\sqrt{2}$	0	0	$-\sqrt{2}$	$\sqrt{2}$	0	0	$\sqrt{2}$	−1
4	1	$-1/\sqrt{2}$	$\sqrt{3/2}$	$-1/\sqrt{2}$	$-\sqrt{3/2}$	$\sqrt{2}$	0	$-1/\sqrt{2}$	$\sqrt{3/2}$	$-1/\sqrt{2}$	$-\sqrt{3/2}$	1
5	1	$-\sqrt{3/2}$	$1/\sqrt{2}$	$1/\sqrt{2}$	$-\sqrt{3/2}$	0	$\sqrt{2}$	$-1/\sqrt{2}$	$-\sqrt{3/2}$	$\sqrt{3/2}$	$1/\sqrt{2}$	−1
6	1	$-\sqrt{2}$	0	$\sqrt{2}$	0	$-\sqrt{2}$	0	$\sqrt{2}$	0	$-\sqrt{2}$	0	1
7	1	$-\sqrt{3/2}$	$-1/\sqrt{2}$	$1/\sqrt{2}$	$\sqrt{3/2}$	0	$-\sqrt{2}$	$-1/\sqrt{2}$	$\sqrt{3/2}$	$\sqrt{3/2}$	$-1/\sqrt{2}$	−1
8	1	$-1/\sqrt{2}$	$-\sqrt{3/2}$	$-1/\sqrt{2}$	$\sqrt{3/2}$	$\sqrt{2}$	0	$-1/\sqrt{2}$	$-\sqrt{3/2}$	$-1/\sqrt{2}$	$\sqrt{3/2}$	1
9	1	0	$-\sqrt{2}$	$-\sqrt{2}$	0	0	$\sqrt{2}$	$\sqrt{2}$	0	0	$-\sqrt{2}$	−1
10	1	$1/\sqrt{2}$	$-\sqrt{3/2}$	$-1/\sqrt{2}$	$-\sqrt{3/2}$	$-\sqrt{2}$	0	$-1/\sqrt{2}$	$\sqrt{3/2}$	$1/\sqrt{2}$	$\sqrt{3/2}$	1
11	1	$\sqrt{3/2}$	$-1/\sqrt{2}$	$1/\sqrt{2}$	$-\sqrt{3/2}$	0	$-\sqrt{2}$	$-1/\sqrt{2}$	$-\sqrt{3/2}$	$-\sqrt{3/2}$	$-1/\sqrt{2}$	−1
12	1	$\sqrt{2}$	0	$\sqrt{2}$	0	$\sqrt{2}$	0	$\sqrt{2}$	0	$\sqrt{2}$	0	1

Table 2. Decadal envelope parameters of sea surface temperature

	Average	Anomaly					
m	1951–80	1951–60	1961–70	1971–80	1981–90	1991–2000	2001–10
Northern Oceanic Region (NOR)							
3	7.23	0.05 ± 0.11*	–0.03 ± 0.16	–0.04 ± 0.04	0.05 ± 0.16	0.15 ± 0.10	0.26 ± 0.11
6	10.95	0.06 ± 0.10	–0.02 ± 0.24	–0.06 ± 0.14	0.02 ± 0.19	0.16 ± 0.27	0.49 ± 0.16
9	14.28	0.09 ± 0.09	–0.02 ± 0.22	–0.15 ± 0.25	0.07 ± 0.25	0.13 ± 0.36	0.57 ± 0.24
12	8.90	0.08 ± 0.10	0.02 ± 0.20	–0.03 ± 0.16	0.12 ± 0.22	0.13 ± 0.18	0.30 ± 0.16
Tropical Oceanic Region (TOR)							
3	26.20	–0.02 ± 0.25	0.03 ± 0.32	0.02 ± 0.31	0.30 ± 0.24	0.45 ± 0.23	0.48 ± 0.24
6	25.97	–0.10 ± 0.25	0.06 ± 0.19	0.02 ± 0.26	0.26 ± 0.20	0.41 ± 0.20	0.49 ± 0.15
9	25.56	–0.09 ± 0.20	–0.02 ± 0.22	0.01 ± 0.25	0.37 ± 0.26	0.41 ± 0.21	0.51 ± 0.15
12	25.80	–0.11 ± 0.28	–0.06 ± 0.29	0.03 ± 0.41	0.29 ± 0.25	0.47 ± 0.34	0.45 ± 0.26
Southern Oceanic Region (SOR)							
3	10.60	–0.13 ± 0.10	–0.07 ± 0.20	0.22 ± 0.17	0.31 ± 0.11	0.32 ± 0.11	0.35 ± 0.08
6	8.25	–0.07 ± 0.17	–0.03 ± 0.21	0.06 ± 0.20	0.21 ± 0.14	0.26 ± 0.10	0.25 ± 0.05
9	7.19	–0.11 ± 0.11	–0.02 ± 0.15	0.15 ± 0.17	0.26 ± 0.08	0.29 ± 0.11	0.29 ± 0.07
12	9.26	–0.15 ± 0.13	–0.04 ± 0.16	0.23 ± 0.17	0.25 ± 0.07	0.26 ± 0.10	0.30 ± 0.13

*The number before ± sign is the coordinate of the decadal envelope centre (ADMM = (decadal maximum + decadal minimum)/2) of SSTA and the number after ± sign is the semi-width (SDMM = (decadal maximum–decadal minimum)/2) of the decadal envelope in °C.

Let over-bar denote 30-year average, here 1951–80, and prime denote anomaly. Then linearity of the eqs (1) and (2) ensures that the coefficient vectors of $\bar{\boldsymbol{T}}$ and $\boldsymbol{T}'_n$ are $\bar{\boldsymbol{c}}$ and $\boldsymbol{c}'_n$. Also

$$\frac{1}{12}\overline{(\boldsymbol{T}^{\mathrm{T}}\boldsymbol{T})} = \bar{c}_1^2 + \sigma^2(\bar{\boldsymbol{T}}) + \overline{(c'_{1n})^2} + \overline{\sigma^2(\boldsymbol{T}'_n)}. \quad (7)$$

The first two terms on the right side depend on the climatological cycle, and the last two depend on variations of the anomaly cycle.

Results

Figure 1 *a* and *b* shows the projections of SSTA trajectories of NOR on solstice and equinox planes. The projection of a decadal envelope on a plane appears as a rectangle with sides parallel to *x*- or *y*-axis. For the sake of clarity, only two such rectangles are shown (1951–60, dashed line; 2001–10, full line). Figure 1 *c*–*f* shows similar trajectories for TOR and SOR, The use of a common scale facilitates comparison between regions and between months.

Table 2 gives the values of two parameters of decadal envelopes of SSTA, namely ADMM (the average of the decadal maximum and the decadal minimum) and SDMM (half of the difference between the decadal maximum and the decadal minimum) for four months. The former is the coordinate of the centre of the decadal envelope, and the latter is its half-width. These geometrical metrics serve as indices of interdecadal and interannual variability.

Let *a* and *s* denote ADMM and SDMM respectively, for a particular decade for a given month, and let a

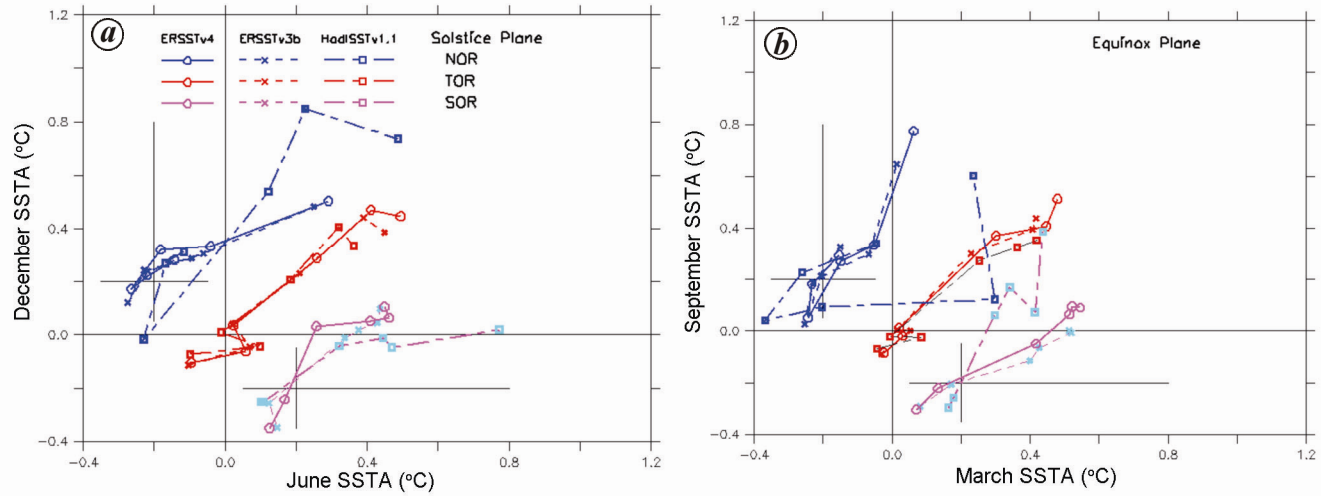

Figure 2 ***a***, ***b***. Projected paths of decadal envelope centres in solstice and equinox planes based on ERSSTv4 (refs 4, 5), ERSSTv3b (ref. 9) and HadISST1.1 (ref. 12). Notation is shown in (***a***). Origin is offset for NOR and SOR for clarity. Paths from the first two databases are in good agreement in all regions. The path from the last database is in fair agreement with that from the first one in TOR, but in NOR and SOR the agreement is limited to first two or three decades.

threshold θ be selected based on the uncertainties. If $a > s + \theta$, then the SST in the given month in any year of the decade exceeds the 1951–80 average for that month by an amount larger than the threshold. In such a case, we may say that the decade is warmer during that month than the 1951–80 average. If such is the case in September or December (March or June), the bottom (left) boundary of the rectangle in Figure 1 *a–f* for that decade would be above (to the right of) the *x*- (*y*-) axis by an amount exceeding θ, which is taken to be 0.1°C in what follows. (Parametric and structural uncertainty in global annual mean SST have been estimated for ERSSTv4 to be less than ~0.02°C and ~0.06°C respectively, for 1951–2010)[5].

Let us examine decadal envelopes for 2001–10 (Figure 1 *a–f*). Since all of them are in the first quadrant and their nearest boundaries are farther from the axes than the threshold, Figure 1 shows that the last decade was warmer than the 1951–80 average in all the three regions in all the four months. The situation is vastly different for 1951–60. It was neither warmer nor cooler than the 1951–80 average in any of the four months in any of the three regions. It can also be seen from Table 2 that the inequality condition is satisfied for all the months and all the regions in the former case and is not satisfied in any month for any region in the latter case.

If SST in 2001–10 is to be compared with that in 1951–60 in a similar way, the preceding criterion has to be modified. Let a and s denote ADMM and SDMM in the first decade and a' and s' in the last decade respectively. If $(a' - a) > (s' + s + \theta)$ for a given month, then we may say that 2001–10 was warmer during that month than 1951–60, in the sense that SST for the month in any year in the last decade would be higher than that for the same month in any year of the first decade by an amount larger than the threshold.

The relative positions of the two rectangles in Figure 1 *a–f*, show that the last decade was warmer than the first decade in SOR in all the four months, except that it was marginally so in June (Figure 1 *e* and *f*, Table 2). On the other hand, it was warmer in TOR and NOR only in June and September (Figure 1 *a–d*). For example, in NOR, $a'–a$ exceeds $s' + s + \theta$ in June (Table 2, 0.43; 0.36) but not in December (Table 2, 0.22; 0.36). Simply put, summer in 2001–10 was warmer than in 1951–60 in NOR, but winter was not.

One interpretation of the above results is that the excess of the SST in 2001–10 over the 1951–80 average is large enough not to be masked by seasonal, interannual or multi-decadal variations in all the regions, but so far as the excess over 1951–60 is concerned, the situation is not uniform. In the case of NOR, the cooling in the first two decades (Figure 1 *a* and *b*) is nearly neutralized by warming in the next two decades. This multi-decadal variation has been identified in numerous studies of Northern Atlantic and Pacific Oceans and designated as Atlantic Multi-decadal Oscillation (AMO) and Pacific Multi-decadal Oscillation (PMO)[14–16].

The ocean surface warming in the last decade relative to 1951–80 climatology has an interesting seasonal feature. The ADMM values in 2001–10 (Table 2) show that the March value of NOR is nearly half of the September value (Figure 1 *a*), and the June value of SOR is nearly two-thirds of the March value (Figure 1 *e* and *f*). Thus ocean surface warming is strongly season dependent in the middle-to-high latitudes, unlike in the low latitudes.

Let us return to the drift trajectories of decadal envelope centre (DEC) shown as black lines connecting circles in Figure 1. A long segment implies a large change in ADMM from previous decade in one or both the months. The longest segments of drift trajectories of DEC in

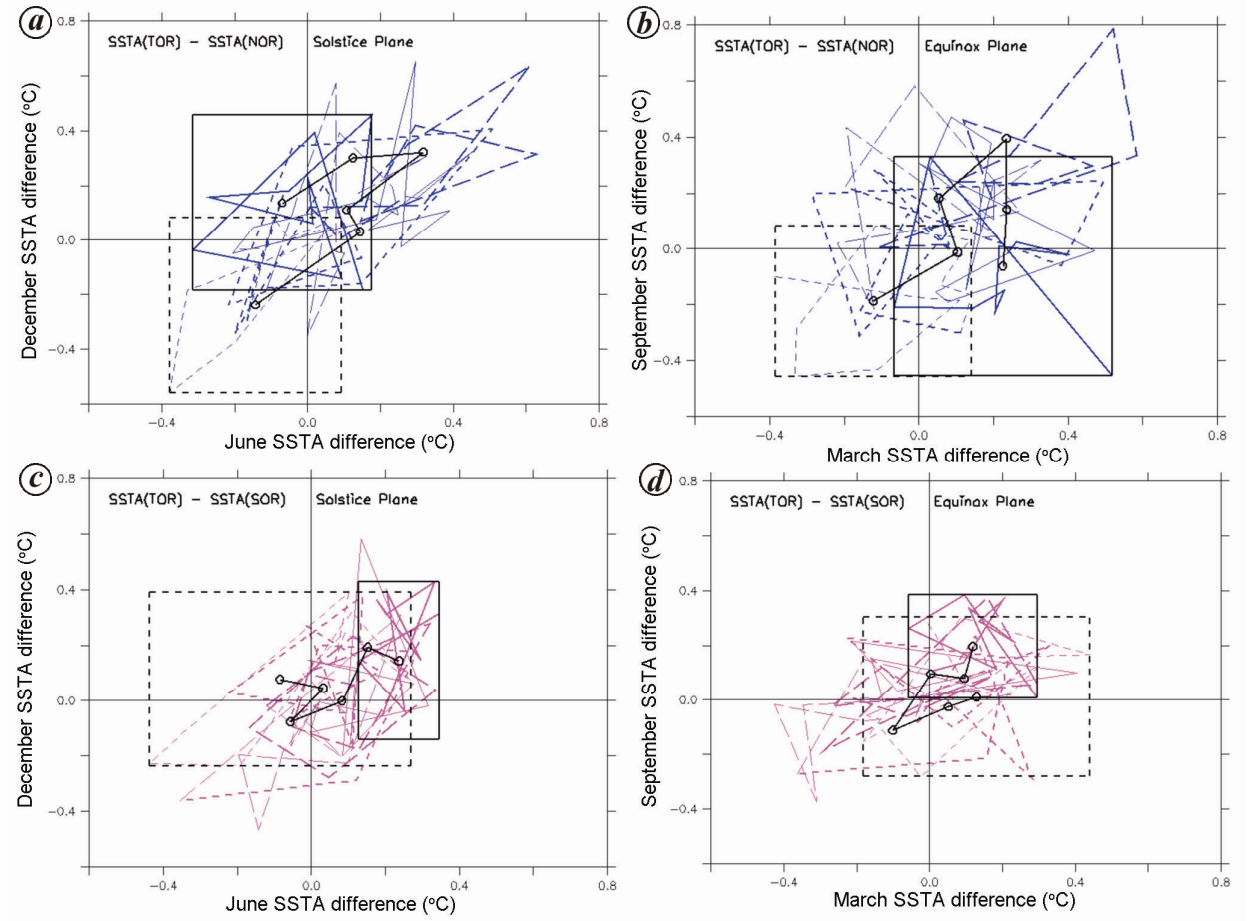

Figure 3 ***a–d.*** Projected trajectories of SSTA of TOR minus SSTA of NOR (blue) or SOR (light blue) in solstice and equinox planes. Remaining notation is as in Figure 1 *a* and *e*. Note that overlapping of dotted and full rectangles suggests a quasibalance on multi-decadal scale and stability of meridional circulation in the atmosphere and the oceans. The decadal envelope parameters are given in Table 3.

Table 3. Decadal envelope parameters of the meridional SST difference

	Average	Anomaly					
m	1951–80	1951–60	1961–70	1971–80	1981–90	1991–2000	2001–10
TOR SST – NOR SST							
3	18.97	–0.12 ± 0.26	0.10 ± 0.39	0.05 ± 0.27	0.23 ± 0.35	0.24 ± 0.23	0.23 ± 0.29
6	15.02	–0.14 ± 0.24	0.14 ± 0.36	0.11 ± 0.22	0.32 ± 0.31	0.12 ± 0.33	–0.07 ± 0.25
9	11.28	–0.19 ± 0.27	–0.01 ± 0.30	0.18 ± 0.40	0.39 ± 0.39	0.14 ± 0.33	–0.06 ± 0.39
12	16.90	–0.24 ± 0.32	0.03 ± 0.37	0.11 ± 0.46	0.32 ± 0.32	0.30 ± 0.35	0.14 ± 0.32
TOR SST – SOR SST							
3	15.60	0.13 ± 0.31	0.05 ± 0.28	–0.10 ± 0.33	0.00 ± 0.29	0.10 ± 0.31	0.12 ± 0.18
6	17.72	–0.08 ± 0.35	0.03 ± 0.25	–0.06 ± 0.30	0.08 ± 0.25	0.15 ± 0.16	0.24 ± 0.11
9	18.37	0.01 ± 0.29	–0.03 ± 0.26	–0.11 ± 0.26	0.10 ± 0.28	0.08 ± 0.14	0.20 ± 0.19
12	16.54	0.08 ± 0.31	0.04 ± 0.33	–0.08 ± 0.39	0.00 ± 0.28	0.19 ± 0.39	0.14 ± 0.28

Figure 1 suggest that the highest decade-on-decade (DoD) increase in ADMM in NOR occurred in 2001–10, in TOR in 1981–90, and in SOR in 1971–80. Also curiously enough, ocean surface in the low latitudes was either a little cooler or a little warmer than in the previous decade (at most 0.1°C) in the decades of highest warming in NOR and SOR.

Before proceeding further, let us compare the DEC trajectories obtained from ERSSTv4 (refs 4, 5) with those obtained from two other datasets, namely ERSSTv3b (ref. 9) and HadISST1.1 (ref. 12). Figure 2 shows projections on solstice and equinox planes of the SSTA trajectories from the three databases. It is noteworthy that despite considerable differences in the data and in the methods,

Table 4. Decadal envelope parameters of warm pool fraction (%) in the tropical oceanic region

	Average	Anomaly					
m	1951–80	1951–60	1961–70	1971–80	1981–90	1991–2000	2001–10
3	17.92	0.00 ± 6.30	1.02 ± 7.15	0.21 ± 7.63	6.82 ± 4.99	11.01 ± 6.52	9.88 ± 5.28
6	20.23	–1.02 ± 5.24	1.82 ± 3.43	0.29 ± 4.04	2.30 ± 5.29	4.94 ± 4.18	6.98 ± 4.21
9	19.48	–1.64 ± 5.42	1.42 ± 4.33	–0.69 ± 5.39	5.87 ± 6.91	7.34 ± 4.40	10.26 ± 2.69
12	11.76	–1.26 ± 2.90	–0.71 ± 4.67	3.02 ± 7.01	5.73 ± 6.12	8.60 ± 7.58	8.72 ± 4.69

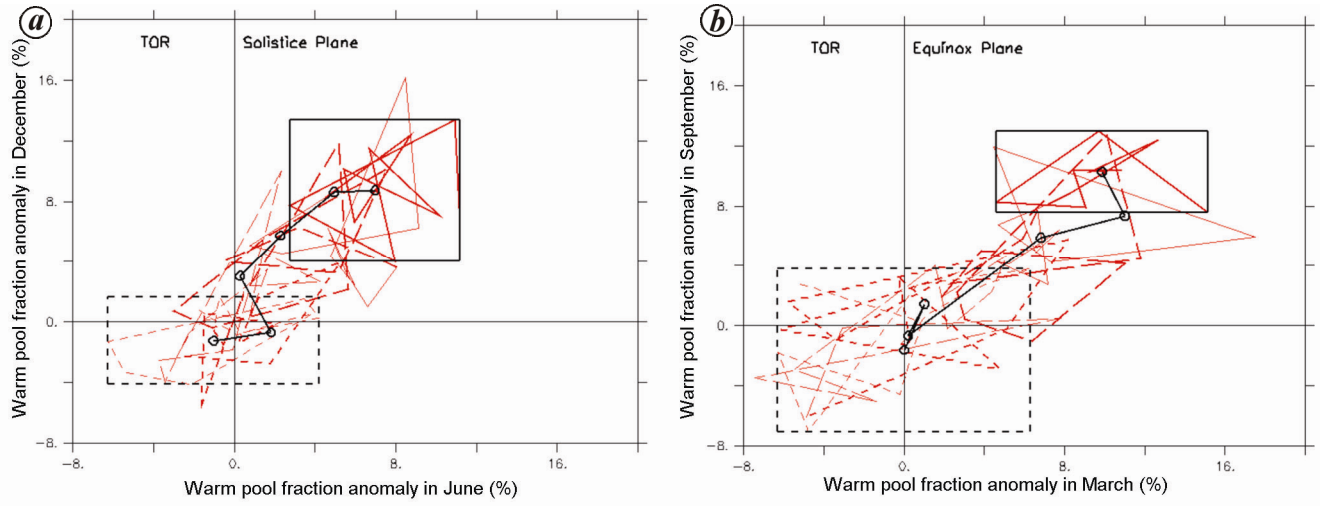

Figure 4 ***a***, ***b***. Projected trajectories of warm pool (SST > 28.5°C) fraction in the TOR in solstice and equinox planes. Notation is as in Figure 1 *c*. Note that the warm pool area has increased significantly over six decades, especially in March and December (Table 4), which indicates greater potential for deep convection and larger advective transport of moisture and latent heat.

there is a fairly good agreement between the three trajectories in TOR. In NOR and SOR, both versions of ERSST are in reasonable agreement. HadISSTv1.1 does show a significantly higher warming tendency, especially in the last decade. This difference is believed to be due to several factors, including reliance of AVHHR data, finer resolution (1° × 1° against 2° × 2°), methods of data analysis as well as bias corrections[4–12].

Differential peaking of the ocean surface warming in the three regions raises the question of the decadal variability of north–south SST difference. Figure 3 shows the trajectories of SSTA difference between TOR and NOR (Figure 3 *a* and *b*) and between TOR and SOR (Figure 3 *c* and *d*). Note that in all the four figures, full-line rectangles have a large overlap with dashed-line rectangles (see also Table 3). Clearly, the general effect of relative changes in the SSTA in low and middle-to-high latitudes appears to be a quasi-balance on a multi-decadal scale between disturbing and restoring changes in meridional SSTA differences. This suggests stability of the global-scale meridional circulation, both atmospheric and oceanic, on multi-decadal scale during 1951–2010.

Large difference in DoD warming tendencies of the ocean surface in low and middle-to-high latitudes in 1971–80 (for SOR) and 2001-10 (for NOR) appears puzzling in view of the globally well-mixed nature of major GHGs, the prime drivers of warming of the earth in recent decades. A plausible explanation for the observed contrasting behaviour is that there was larger-than-normal heat transfer in those two decades from the low latitudes to the middle-to-high latitudes either through the atmosphere or the ocean, or both. Another possible explanation is larger-than-normal heat transfer to intermediate or deeper waters. The second mechanism prima facie appears less likely as increasing SST tends to have a stabilizing effect on the seawater below and a destabilizing effect on the air above.

To explore the possibility of such heat transfer through the atmosphere, let us examine the projected trajectories of anomaly of warm pool fraction (the percentage of area of TOR where monthly mean SST > 28.5°C) in the solstice and equinox planes. These trajectory projections (Figure 4 *a* and *b*, Table 4) show that ADMM of warm pool area fraction has increased, on an average, between ~1% and ~2% per decade depending on the season. Hence increasingly larger areas of the ocean in the low latitudes have acquired the potential of sustaining deep convection in the atmosphere.

It is therefore reasonable to hypothesize that increased deep convection in the low latitudes results in greater

Table 5. Parameters of annually modulated normal modes of SSTA

	Average	Anomaly					
Parameter	1951–80	1951–60	1961–70	1971–80	1981–90	1991–2000	2001–10
NOR							
c_1	10.35	0.09 ± 0.07	0.00 ± 0.15	–0.10 ± 0.10	0.06 ± 0.19	0.15 ± 0.19	0.41 ± 0.12
$\sqrt{2}r_1$*10	37.09	0.48 ± 0.63	0.19 ± 1.17	–0.45 ± 1.21	–0.28 ± 0.93	–0.13 ± 1.92	1.80 ± 1.24
$\sqrt{2}r_2$*10	7.02	0.20 ± 0.36	–0.09 ± 0.78	0.30 ± 0.56	–0.19 ± 0.47	0.05 ± 0.35	0.12 ± 0.38
$\sqrt{2}r_3$*10	1.33	0.06 ± 0.40	0.02 ± 0.30	0.00 ± 0.27	–0.04 ± 0.23	0.16 ± 0.44	0.00 ± 0.42
ϕ_1	–108.3	0.3 ± 0.5	0.0 ± 1.2	–0.6 ± 2.0	0.2 ± 0.7	0.3 ± 1.1	–0.1 ± 1.1
ϕ_2	63.3	0.7 ± 1.1	0.0 ± 1.8	–0.7 ± 2.7	0.6 ± 1.3	0.6 ± 1.2	–0.2 ± 2.1
ϕ_3	1.7	–0.2 ± 6.3	0.9 ± 4.3	–1.1 ± 5.8	1.5 ± 5.8	–1.5 ± 4.4	–1.7 ± 4.7
$\lvert\varepsilon_2\rvert$*100	10.1	0.1 ± 3.0	0.7 ± 2.6	–0.5 ± 2.0	–0.1 ± 1.8	1.4 ± 3.2	–0.4 ± 2.9
$\lvert\varepsilon_3\rvert$*100	3.4	0.6 ± 2.6	0.9 ± 2.1	–0.2 ± 2.3	0.2 ± 1.3	0.8 ± 0.9	0.1 ± 1.6
TOR							
c_1	25.88	–0.09 ± 0.24	0.07 ± 0.19	0.02 ± 0.24	0.29 ± 0.20	0.38 ± 0.17	0.46 ± 0.11
$\sqrt{2}r_1$*10	3.40	–0.39 ± 1.19	–0.36 ± 1.95	–0.31 ± 1.77	0.11 ± 1.45	–0.48 ± 2.13	0.37 ± 1.80
$\sqrt{2}r_2$*10	1.71	0.03 ± 0.74	–0.09 ± 0.77	0.11 ± 0.90	0.01 ± 0.52	0.18 ± 0.98	–0.06 ± 0.76
$\sqrt{2}r_3$*10	0.34	–0.08 ± 0.16	0.10 ± 0.30	0.13 ± 0.36	0.04 ± 0.26	0.01 ± 0.33	0.03 ± 0.28
ϕ_1	104.5	4.2 ± 12.1	1.8 ± 7.1	–0.8 ± 14.3	–1.3 ± 10.1	1.3 ± 9.4	3.9 ± 16.0
ϕ_2	–45.4	0.2 ± 7.2	–2.5 ± 11.9	–5.5 ± 13.4	–6.2 ± 13.7	2.9 ± 6.7	1.6 ± 7.4
ϕ_3	18.4	–3.3 ± 38.6	–13.3 ± 47.5	1.2 ± 39.6	–15.6 ± 47.8	–13.3 ± 54.0	–20.4 ± 48.8
$\lvert\varepsilon_2\rvert$*100	3.9	–0.9 ± 2.0	0.9 ± 3.4	1.4 ± 3.7	0.4 ± 2.4	1.5 ± 4.0	–0.3 ± 2.6
$\lvert\varepsilon_3\rvert$*100	2.9	–0.3 ± 1.9	0.4 ± 3.0	1.1 ± 2.9	0.3 ± 1.6	1.6 ± 3.5	–0.3 ± 1.8
SOR							
c_1	8.82	–0.11 ± 0.09	–0.07 ± 0.11	0.20 ± 0.13	0.26 ± 0.06	0.29 ± 0.08	0.31 ± 0.06
$\sqrt{2}r_1$*10	17.96	–0.51 ± 0.53	0.16 ± 0.99	0.37 ± 0.63	0.44 ± 0.40	0.55 ± 0.61	0.44 ± 0.37
$\sqrt{2}r_2$*10	2.21	–0.29 ± 0.72	0.09 ± 0.72	–0.17 ± 0.65	0.28 ± 0.44	0.06 ± 0.49	0.21 ± 0.68
$\sqrt{2}r_3$*10	0.39	0.02 ± 0.20	0.04 ± 0.30	–0.10 ± 0.24	0.03 ± 0.23	–0.04 ± 0.30	–0.08 ± 0.26
ϕ_1	72.5	0.7 ± 3.7	–0.8 ± 3.1	–1.6 ± 2.0	0.3 ± 2.6	0.9 ± 1.4	0.5 ± 1.4
ϕ_2	54.1	–1.6 ± 7.1	0.6 ± 8.8	1.9 ± 5.0	1.5 ± 5.5	1.7 ± 4.7	1.9 ± 4.7
ϕ_3	20.4	–21.5 ± 58.3	–17.6 ± 16.9	–15.3 ± 51.3	19.3 ± 16.7	18.1 ± 17.4	21.5 ± 10.6
$\lvert\varepsilon_2\rvert$*100	4.2	0.2 ± 1.5	0.8 ± 2.2	–0.7 ± 2.4	–0.8 ± 1.7	–1.2 ± 1.8	–1.2 ± 1.8
$\lvert\varepsilon_3\rvert$*100	3.1	0.3 ± 1.3	0.4 ± 1.6	–0.3 ± 1.9	–1.5 ± 0.6	–1.7 ± 0.8	–1.6 ± 1.3

c_1, r_k, ϕ_k and $|\varepsilon_K|$ are the annual mean, the normalized amplitude and the phase of the kth mode and the magnitude of the error for the Kth mode approximation (k = 1, 2, 3; K = 2, 3). Phase is in degrees and the rest in °C (see Appendix 1).

transport of moisture to middle and upper troposphere from where a part of it is advected to the middle-to-high latitudes. Such transport would have two effects: one, increased GHG effect till the moisture returns to the earth surface as rain or snow; second, increased albedo as long as the snow does not melt. The first effect enhances warming in summer and fall, and the second limits warming in winter.

In order to examine the effect of warming on the annual cycle, it is expedient to move to the frequency domain. AMNMs were introduced in the previous section to extend Fourier analysis of climatological cycle to annual cycle. It is sufficient to consider four major modes, namely annual mean and the first three regular modes (k = 1, 2, 3 cy^{-1}), as they account for bulk of the annual variance. Table 5 gives the values of their parameters. As explained in Appendix 1, approximations based on them can give an accuracy of ~0.03°C.

Although semi-annual and the four-month mode contribute significantly to the annual variance, decadal variations in ADMM and SDMM of their amplitudes are less than 0.1°C. So we focus attention only on decadal variations of annual mean anomaly and amplitude anomaly of the annual mode. In Figure 5 *a* and *b*, their ADMM and SDMM values are shown for six decades (Amplitude, as traditionally defined, is $\sqrt{2}$ times the normalized amplitude r_{kn}, $1 \le k \le 5$).

The variation of ADMM of these two parameters for SOR (Figure 5 *a* and *b*, light blue circles) clearly suggests a transition from one equilibrium state to another with a higher annual mean (~0.4°C) and a higher amplitude anomaly (~0.1°C) of the annual mode. The transition seems to have occurred in the second or third decade, and is followed by gradual relaxation.

Similarly, variation of these two parameters for NOR (Figure 5 *a* and *b*, blue circles) suggests a transition from a multi-decadal oscillatory state to another oscillatory state. It has started in the last two decades, but it is not clear whether the new oscillatory state has been attained. But if one assumes that it is close to the new state, it has

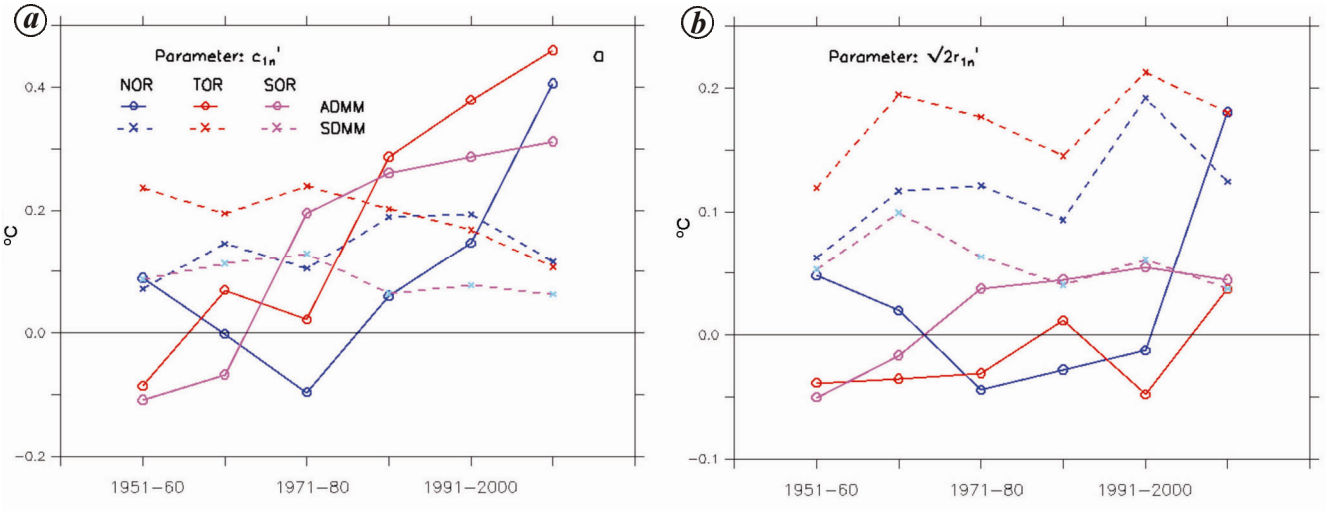

Figure 5. Decadal variations of parameters of annually modulated normal modes in 1951–2010: (***a***) annual mean anomaly, and (***b***) amplitude anomaly of annual mode. The centre of decadal envelope is given by ADMM (=[decadal maximum + decadal minimum]/2) and its semi-width by SDMM (=[decadal maximum – decadal minimum]/2). Note DoD growth of ADMM of the annual mean has peaked in SOR, TOR and NOR in 1971–80, 1981–90 and 2001–10 respectively.

a higher annual mean (~0.3°C) and a higher amplitude anomaly (~0.2°C) of the annual mode.

Interpretation of similar variations of ADMM and SDMM in TOR is difficult because of a decadal-scale oscillatory perturbation, which may be attributed to Pacific Decadal Oscillation. A transition seems to be in progress over all the six decades. The new state could end up having its ADMM of annual mean at least ~0.5°C higher than the earlier one.

Discussion

Let us discuss the hypothesis of increased atmospheric transport of moisture from TOR. It is but natural to ask whether there is any independent evidence supporting such a hypothesis.

Adikari and Yoshitani[17] have analysed the data of the Emergency Events Database (EMDAT, http://www.emdat.be) maintained at the University of Catholic Louvain, Belgium. Out of the 11 categories of natural disasters, more than half of the disasters recorded during 1900–2006 were either floods or windstorms. The growth rate of floods increased from ~50% per decade in the period 1980–82 to 1995–97 to ~130% per decade in the period 1995–97 to 2004–06, and the growth rate of storms from 30% to 50% per decade[16]. These data suggest increased moisture and energy in the atmosphere and that the warm-pool areas in TOR are prime candidates for being their source.

Rutgers University Global Snow Lab, NJ, USA publishes on-line monthly snow cover extent (SCE) data starting from 1967. It is interesting that SCE anomalies in the northern hemisphere in January and February have exceeded 1 million sq km for nearly half of the years between 2001 and 2016 (ref. 18). This is a clear indication of increased advective transport of moisture from the low latitudes in the last few years.

It should however be stressed that modelling and observational investigations are needed to test the validity of the hypothesis as well as to determine the changes in the atmospheric and oceanic circulation on regional and sub-regional scales that accompany increased advective transport of moisture and latent heat.

Although the preceding discussion stresses the role of advective atmospheric transport, advective oceanic transport is also important. It takes place mainly through western boundary currents, e.g. Kuroshio Current and the Gulf Stream in the northern hemisphere. The strength of these boundary currents depends on the location of the point where the North or South Equatorial Current bifurcates on reaching the coast. There is evidence to show that this bifurcation point has moved over 60 years, suggesting a multi-decadal variation in the northward or southward flow[19] and consequently multi-decadal variation of the oceanic heat transport from TOR.

Conclusion

The time and frequency domain methods of SST state space introduced here lead to the following major findings:

1. The warming of the ocean surface varies with season in the middle-to-high latitudes unlike in the low latitudes (Figure 1 and Table 2). This implies that decadal-scale warming affects the annual cycle in NOR and SOR. Indeed, increase in the annual mean anomaly is accompanied by increase in the amplitude anomaly of the annual mode in NOR and SOR (Figure 5 and Table 5).

Appendix 1.

Additional notes on the method

1. The matrix **F** given in Table 1 is a special case of a class of $2K \times 2K$ matrices ($K > 1$) whose elements are given by

$$F_{ij} = 1, \text{ if } j = 1,$$

$$F_{ij} = \sqrt{2}\cos\left(\frac{ik\pi}{K}\right), \text{ if } j = 2k < 2K,$$

$$F_{ij} = \sqrt{2}\sin\left(\frac{ik\pi}{K}\right), \text{ if } j = 2k + 1 < 2K,$$

$$F_{ij} = (-1)^i, \text{ if } j = 2K.$$

Clearly, $\mathbf{F}^{\mathrm{T}}\mathbf{F} = 2K\mathbf{I}$. Several values of K are potentially useful (e.g. $K = 2$ for quarterly analysis, $K = 12$ for hourly analysis of diurnal cycle and $K = 73$ for pentad based analysis in meteorological applications with a two-year period.).

2. Two and three-mode approximations of annual cycle. A common approximation of the climatological cycle retains two regular modes (annual and semi-annual), along with the annual mean. If a similar approximation is used for annual cycles in TOR and SOR, it would be accurate to within ~0.04°C (Table 5, $K = 2$). If it is used for NOR, the average error would be ~0.1°C. So it seems preferable to use three-mode approximation, which would give an accuracy of ~0.03°C (Table 5, $K = 3$).

2. SSTA difference between TOR and NOR or SOR has remained stable on multi-decadal time scale (Figure 3 and Table 3), indicating multi-decadal stability of global meridional circulation in the atmosphere and the ocean.

3. Decadal envelope drift of warm pool fraction in the TOR has increased, on an average by ~1% to ~2% per decade depending on the season (Figure 4 and Table 4). Therefore, if this trend continues, we should expect further increase on a decadal scale in the moisture and latent heat in the troposphere in TOR, and in the potential for their advective transport to middle-to-high latitudes.

1. Gill, A. E., *Atmosphere-Ocean Dynamics*, Academic Press, London, 1982, pp. 2–3.
2. Marshall, J. and Plumb, R. A., *Atmosphere, Ocean, and Climate Dynamics: An Introductory Text*, Elsevier, Amsterdam, 2008, pp. 63–64.
3. Yajnik, K., Analysis of 150 years of sea surface temperature data using discretely modulated modes. In Abstracts, International Conference on 'Computational and Data Intensive Science', CSIR Fourth Paradigm Institute, Bengaluru, 26–28 August 2013, pp. 10–14.
4. Huang, B. *et al.*, Extended Reconstructed Sea Surface Temperature version 4 (ERSST.v4). Part I: upgrades and intercomparison. *J. Climate*, 2015, **28**, 911–930; doi: 10.1175/JCLI-D-14-00006.1.
5. Liu, W. *et al.*, Extended Reconstructed Sea Surface Temperature version 4 (ERSST.v4). Part II: parametric and structural uncertainty estimation. *J. Climate*, 2015, **28**, 931–951; doi: 10.1175/JCLI-D-14-00007.1.
6. Smith, T. M. and Reynolds, R. W., Extended reconstruction of global sea surface temperatures based on COADS data (1854–1997). *J. Climate*, 2003, **16**, 1495–1510.
7. Smith, T. M. and Reynolds, R. W., Improved extended reconstruction of SST (1854–1997). *J. Climate*, 2004, **17**, 2466–2477.
8. Smith, T. M. and Reynolds, R. W., A global merged land–air–sea surface temperature reconstruction based on historical observations (1880–1997). *J. Climate*, 2005, **18**, 2012–2036.
9. Smith, T. M. *et al.*, Improvements to NOAA's historical merged land–ocean surface temperature analysis (1880–2006). *J. Climate*, 2008, **21**, 2283–2296.
10. Smith, T. M. and Reynolds, R. W., Bias corrections for historical sea surface temperatures based on marine air temperatures. *J. Climate*, 2002, **15**, 73–87.
11. Reynolds, R. W. *et al.*, An improved in situ and satellite SST analysis for climate. *J. Climate*, 2002, **15**, 1609–1625.
12. Rayner, N. A. *et al.*, Global analyses of sea surface temperature, sea ice, and night marine air temperature since the late nineteenth century. *J. Geophys. Res.*, 2003, **108**, 4407; doi: 10.1029/2002JD002670.
13. Rao, R. R., Molinari, R. L. and Festa, J. F., Evolution of the climatological near-surface thermal structure of the Indian Ocean. *J. Geophys. Res.*, 1989, **94**, 10801–10815.
14. Schlesinger, M. E. and Ramankutty, N., An oscillation in the global climate system of period 65–70 year. *Nature*, 1994, **367**, 723–726.
15. Delworth, T. L. and Mann, M. E., Observed and simulated multidecadal variability in the Northern Hemisphere. *Climate Dyn.*, 2000, **16**, 661–676.
16. Steinman, B. A., Mann, M. E. and Miller, S. K., Atlantic and Pacific multidecadal oscillations and northern hemisphere temperatures. *Science*, 2015, **347**, 988–991.
17. Adikari, Y. and Yoshitani, J., Global trend in water-related disasters: an insight for policymakers. UNESCO, Paris, France, 2009.
18. http://climate.rutgers.edu/snowcover/chart_anom.php?ui_set=1&ui_region=nhland&ui_month=1 or 2.
19. Hu, D. *et al.*, Pacific western boundary currents and their roles in climate. *Nature*, 2015, **522**, 299–308; doi: 10.1038/nature14504.

ACKNOWLEDGEMENTS. I thank Shyam Chetty and Prof. P. Seshu, both former Scientist-in-Charge, CSIR-4PI for the use of the Institute facilities; Prof. V. K. Gaur and Dr P. S. Swathi, CSIR-4PI for helpful suggestions; K. Devasana for datasets-related assistance, and M. K. Sharada, R. P. Thangavelu, CSIR-4PI and G. Nagaraju, formerly of CSIR-4PI for help.

Received 30 November 2015; revised accepted 14 April 2016

doi: 10.18520/cs/v111/i5/843-852